

Integrated Rock Characterization of Tight Reservoir by Multiple Analytical Techniques*

Omprakash Pal¹, Waseem Abdulrazzaq¹, Rachad Zeriek¹, Amr Ibrahim¹, and Mohamed Awad¹

Search and Discovery Article #41921 (2016)**

Posted October 31, 2016

*Adapted from extended abstract prepared in relation to poster presentation given at GEO 2016, 12th Middle East Geosciences Conference & Exhibition, Manama, Bahrain, March 7-10, 2016

**Datapages © 2016. Serial rights given by author. For all other rights contact author directly.

¹Halliburton, Al-Khobar, Saudi Arabia (Waseem.abdulrazzaq@halliburton.com)

Abstract

Tight gas reservoirs contain a variety of formations, such as shale gas, tight sandstone, and carbonates, etc. Many of these reservoirs are very complex in terms of mineralogical composition and petrophysical properties; consequently, the hydraulic properties are not simple and straightforward. The mineralogical compositions are complex because of varying amounts of quartz, calcite, dolomite, feldspar, and clay. The type and nature of clay content present between the pores greatly affects petrophysical properties. Therefore, an integration of geological and petrophysical properties are very crucial to gaining an understanding of the reservoir and optimizing the development strategy.

This article discusses rock characterization of formation samples using multiple analytical instruments, such as X-ray fluorescence (XRF), X-ray diffraction (XRD), and qualitative evaluation of minerals by scanning electronic microscope (QEMSCAN). The XRF determines the elemental composition of formation, and XRD determines the mineralogical composition of formation based on international center for diffraction data (ICDD) database and regression method using external standards. QEMSCAN is used for spatial distribution of individual minerals and textural variations, porosity distribution, and grain density within rock samples. The presence of swelling clays in a formation leads to swelling upon contact with water. Swelling clay content is estimated by cation exchange capacity and correlated with XRD mineralogical analysis.

The compilation of data from diverse techniques helps present a complete picture of lateral heterogeneity in unconventional reservoirs, which ultimately helps improve designing formulation for fracturing fluid and drilling fluids to help prevent non-productive time (NPT).

Introduction

The industry supply and demand for hydrocarbon has increased and is anticipated to intensify further, particularly in the Middle East. This has enhanced emphasis on exploration and development of unconventional reservoirs, specifically tight sandstones, tight carbonates, and highly

heterogeneous tight shales. In fact, unconventional reservoirs are known for preserving huge amounts of hydrocarbon and, at the same time, these reservoirs do not produce economically (Passey et al., 2010). A specially designed stimulation technique based on hydraulic fracturing fluid and proppant was used to exploit such reservoirs and makes it feasible to produce economically. The huge unconventional resources have already been explored in North America, such as Barnett, Haynesville, Woodford, Eagleford, Marcellus, and Fayetteville (Ronger, 1997; Hill et al., 2004; Perry and Lee, 2007) and the Montney and Horn River in Canada, Eastern Europe, Russia, China (Lu et al. 2012), Australia, and Saudi Arabia (Alexeyenko et al., 2013; Hayton, et al. 2010; Sahin, 2013, Ali et al., 2013).

Sandstone, shale, and carbonates are sedimentary rocks; they are considered where permeability values are less than 0.01md (Smith et al., 2013). Sandstones are primarily composed of quartz, feldspar, and rock fragments, whereas shales are sedimentary rocks dominantly consisting of clay minerals with varying percentages of quartz, calcite, feldspar, pyrite, and hydrocarbons. Shale rocks are highly heterogeneous in terms of petrophysical properties and mineralogy, including type and amount of clays present in and between pores. Understanding complex shale formations under high resolution analytical state-of-the-art equipment leads to better understanding of tight reservoirs and eventually can help improve hydrocarbon (oil and gas) production. The sedimentological and petrophysical properties for each unconventional reservoir greatly differ from basin to basin.

Previously, the copy-paste rule of thumb for drilling and completion phases was used for developing unconventional shale reservoir or, in other words, trial and error methods. This variation is attributed to the heterogeneous nature of shale reservoirs, rather than technology. Keeping such scenarios in view, a systematic work has been designed to characterize, understand, predict, and develop such complex reservoirs. The methods ultimately reduce NPT cost, and resources ([Figure 1](#)).

This article focuses on integrated characterization techniques, such as XRD, XRF, and QEMSACN, to better understand mineralogy, mineral distribution, and porosity. Different reservoir rock samples, such as quartz-rich samples, carbonate-based, and shale samples, have been selected for integrated characterization. This article discusses XRF used for elemental characterization, XRD for mineralogical composition, and QEMSAN to determine the automated mineralogy along with pore size, density, and grain-size distribution. Each test and its respective results are discussed.

XRF Analysis

An XRF spectrometer is used for routine chemical analyses of rocks, minerals, sediments, and fluids. In the present study, the formation rock samples were crushed and ground to approximately 5 micron particle size, and then made into pressed pellets using binder for XRF measurement: measured XRF using energy dispersive XRF spectrophotometer. The concentration of elements was determined against the standard calibration curve and reported in their respective oxide form. XRF results are reported later.

XRD Analysis

XRD is normally used to determine mineralogy of reservoir rocks. Few grams of specimen were crushed, ground, and passed through 200-mesh sieves to attain uniform grain size particles. A powdered sample was scanned between 2 to 80 theta under X-ray to obtain the diffraction

pattern to semi-quantify the mineralogical composition. Each peak on acquired XRD spectrum corresponds to a particular mineral ([Figure 2](#)) and was analyzed using the ICCD library, whereas relative abundance of each mineral was determined by relative intensity ratio. Shale samples containing a significant quantity of clay can be further analyzed by XRD analysis of a glycolated slide to determine each clay fraction, such as illite, smectite, kaolinite, and chlorite.

Formation samples containing swelling clay when titrated with methylene blue readily adsorbs methylene blue dye because of the cation exchange capacity phenomena. Determination of cation exchange capacity of formation provides information about their reactivity to water and estimation of swelling clay concentration. In the present study, methylene blue testing was also performed to determine the cation exchange capacity of formation samples.

QEMSCAN Analysis

QEMSCAN is a highly sophisticated state-of-the-art machine used to scan the rock sample and acquire photo-micro-images. These photo-micro-images are framed together and stitched to form a mosaic that represents the entire rock-sample's surface. Individual pixels of photomicrographs provide elemental information, which is represented by means of spectrum used to derive minerals, along with spatial distribution within the unit area of study (i.e., mineral distribution map). Each pixel is color-coded to display the elemental and mineral distribution.

Sample Preparation for QEMSCAN Analysis

The core plug and cutting samples were mounted in high-viscosity, fast-curing epoxy using 30-mm molds to help ensure a random and homogeneous distribution of particles. The 30-mm blocks were sectioned perpendicular to the C axis to expose a representative surface. The sectioned blocks were grinded and mechanically polished. Because minerals in sedimentary rocks have a high resistance or are insulators, it is important to help prevent charging effects by coating the sample with a thin conductive layer. To achieve this, a thin layer of carbon was applied. Carbon is a light element resulting in a low absorption for secondary and backscattered electrons, but still has an acceptable conductivity when applied to even and polished surfaces.

QEMSCAN data and images are represented in [Figures 3, 4, and 5](#). Backscattered images were also collected to determine the automated mineral density represented in [Figures 6 and 7](#). Grain sizes of clastic rocks were also determined from QEMSCAN and are presented in [Figures 8 and 9](#).

Results and Discussions

Samples 1 through 4 are rich in quartz with substantial quantities of clays illite and kaolinite. QEMSCAN, XRD, and XRF data are given in [Figures 3 and 4](#). The major clay minerals determined by XRD are in line with QEMSCAN and with major elemental composition determined using XRF. In XRD patterns, illite and muscovite appears at 2 theta at approximately 8.9°. Illite gives little broader peak than muscovite and

can overlap muscovite and therefore might not be discriminated by XRD. However, QEMSCAN distinguished the illite and muscovite in Samples 1 through 4.

Porosity is the volumetric void space (i.e., the space not occupied by solid material). The determination of porosity is of great importance because it determines the ultimate volume of a rock type that could contain hydrocarbon. Pore percentages of Samples 1 through 4 are less than 10 in all samples, indicating tight sand.

[Figures 5](#) and [6](#) show QEMSCAN, XRD, and XRF data of Samples 5 and 6. It is evident from [Figures 5](#) and [6](#) that Sample 5 and 6 are carbonate-rich. Sample 5 contains 99% carbonate with an approximately similar percentage of dolomite and calcite. Sample 6 comprises primarily dolomite along with gypsum (anhydrite). Mineralogy determined using XRD and QEMSCAN are qualitatively similar and well supported by the major elemental concentration determined using XRF.

The pore percent of Sample 6 is 1.14% (tight carbonate) and is slightly higher compared to Sample 5. Dolomite content in Sample 6 is higher than in Sample 5, which is known for higher secondary porosity.

Samples 7 and 8 are clay-rich samples and primarily contain kaolinite, illite, illite/smectite mixed-layer, and chlorite along with quartz. Chlorite and mixed-layer are evident by XRD but not detected by QEMSCAN. The major minerals determined by XRD and QEMSCAN are similar, except chlorite and mixed-layer. The mineralogical composition determined by XRD and QEMSCAN are well supported by elemental composition determined by XRF. Identification and determination of the swelling clay content in any shale sample are of prime importance as it decides the potential of shale reactivity with water. Shale samples containing a high percentage of swelling clay, such as smectite and smectite/mixed-layers, require a clay-swelling inhibitor in drilling fluid while drilling and in fracturing fluid during hydraulic fracturing.

The pore percentage of both Samples 7 and 8 is very low because it is tight shale. However, the pore percentage of Sample 7 is 1.16% and is slightly higher than Sample 8, which has a pore percentage of 0.48. This might be attributed to a more prominent fracture in Sample 7, which is evident from the QEMSCAN image of Sample 7.

Sample density has been determined by backscattered electron (BSE) images of QEMSCAN. BSE images of Samples 1 through 4, given in [Figures 7](#) and [8](#), represents BSE images of Samples 5 through 8. Samples 5 and 6 are carbonate-based samples and show a higher density than the quartz and shale samples.

QEMSCAN was also used to determine the grain-size distribution of formation samples. Grain-size distributions of samples are represented in [Figure 9](#). Samples containing higher quartz content have a larger grain size than shale and carbonate samples.

Based on the discussed analytical techniques, it is evident that one technique might not be sufficient to provide a detailed understanding of reservoir rock; so, multiple analytical techniques are necessary to achieve integrated and detailed knowledge about the formation heterogeneity.

Conclusions

This article discussed the characterization of three primary types of rocks using state-of-the-art analytical instruments. Results acquired from these techniques are in line with each other and considered very helpful in making analysis and decisions. In general, harmony among XRD, XRF and QEMSCAN have been observed to specify major clays and non-clays minerals in sandstone and shale formations. Integration of these techniques also help identify calcite from dolomite and their spatial distribution within the rocks.

Each analytical technique has merits and demerits. XRF provides an elemental concentration of samples, and mineralogical composition can be determined based on theoretical calculation. However, it cannot discriminate between the minerals having the same chemical composition but different crystalline structure (e.g., calcite, vaterite, and aragonite).

XRD provides information about the crystalline material only. Amorphous material does not provide XRD patterns and is not detectable using XRD.

QEMSCAN helps identify mineralogical mapping, pore percentage, and grain-size distribution. Geospatial distribution of each and every mineral in each individual rock type can be represented by means of color-coding.

Based on the discussed analytical techniques, it is evident that one technique might not be sufficient to provide the necessary detailed understanding of the reservoir rock; therefore, multiple analytical techniques can help integrate details regarding the formation heterogeneity.

Selected References

Alexeyenko A.V., K.M. Bartko, I.A. Adebisi, et al., 2013, First shale gas experience in Saudi Arabia -Lessons learned: *Journal of Engineering Research*, v. 1/2, p. 29–42.

Hayton, S., C. Heine, and B.E. Gratto, 2010, Tight gas exploration in Saudi Arabia: SPE-131065-MS (presented at the SPE Deep Gas Conference and Exhibition, Manama, Bahrain, 24–26 January). Website accessed October 11, 2016, <http://dx.doi.org/10.2118/131065-MS>.

Hill D.G., T.E. Lombardi, and J.P. Martin, 2004, Fractured shale gas potential in New York: *Northeastern Geology and Environmental Sciences*, v. 26/1-2, p. 57–58.

Lu, S., W. Huang, W. Li, D. Xiao, J. Li, W. Wang, M. Wang, F. Chen, S. Deng, and Z. Tang, 2015, Lower limits and grading evaluation criteria of source rocks and reservoirs of tight oil and gas: *Acta Geologica Sinica (English version)*, v. 89/1, p. 67-70. Website accessed October 12, 2016, http://onlinelibrary.wiley.com/doi/10.1111/1755-6724.12302_29/full.

Pal, O., B. Zoghbi, and W. Razzaq, 2015, Characterization of unconventional reservoir for development and production: An integrated approach: SPE-172919-MS (presented at the SPE Middle East Unconventional Resources Conference and Exhibition, Muscat, Oman, 26–28 January). Website accessed October 11, 2016, <http://dx.doi.org/10.2118/172919-MS>.

Passey, Q.R., K. Bohacs, W.L. Esch, et al., 2010, From oil-prone source rock to gas-producing shale reservoir—Geologic and petrophysical characterization of unconventional shale gas reservoirs: SPE-131350-MS (presented at the International Oil and Gas Conference and Exhibition, Beijing, China, 8–10 June). Website accessed October 12, 2016, <http://dx.doi.org/10.2118/131350-MS>.

Perry, K., and J. Lee, 2007, Unconventional Gas Reservoirs—Tight Gas, Coal Seams, and Shales: Working Document of the NPC Global Oil and Gas Study, Topic Paper #29, 54p. Website accessed October 11, 2016, http://www.npc.org/Study_Topic_Papers/29-TTG-Unconventional-Gas.pdf.

Rogner, H-H., 1997, An Assessment of World Hydrocarbon Resources: Annual Review of Energy and the Environment, v. 22, p. 217-262. Website accessed October 11, 2016, <http://www.annualreviews.org/doi/10.1146/annurev.energy.22.1.217>.

Sahin, A., 2013, Unconventional natural gas potential in Saudi Arabia: SPE-164364-MS (presented at SPE Middle East Oil and Gas Show and Exhibition, Manama, Bahrain, 10-13 March). Website accessed October 12, 2016, <https://www.onepetro.org/conference-paper/SPE-164364-MS>.

Smith C.H., S. Ramakrishna, and J. Bray, 2013, Magnetic resonance to identify permeability in shale reservoirs: SPE-166992-MS (presented at the SPE Unconventional Resources Conference and Exhibition-Asia Pacific held in Brisbane, Australia, 11–13 November). Website accessed October 12, 2016, <http://dx.doi.org/10.2118/166992-MS>.

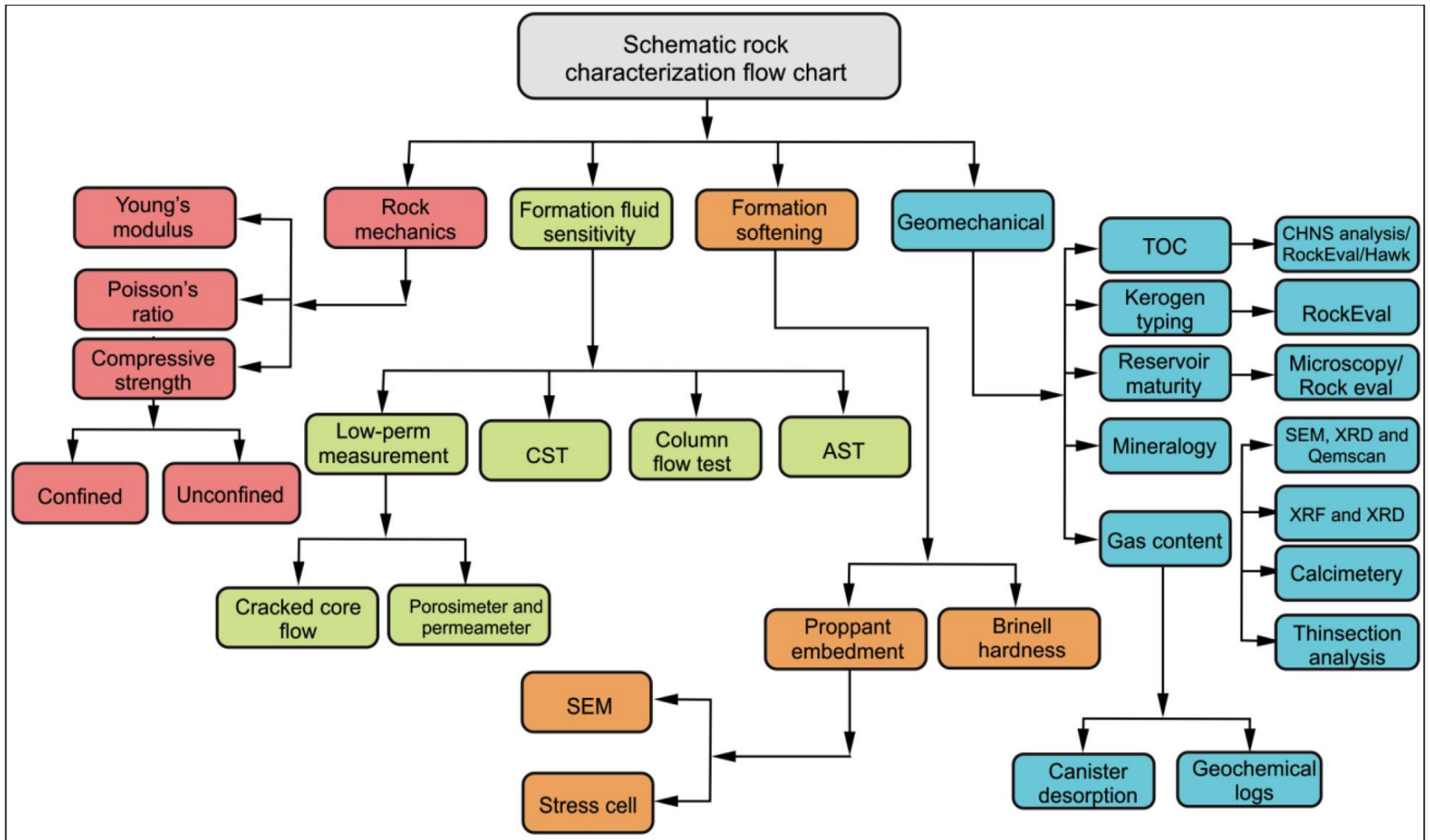


Figure 1. Flow diagram of the shale evaluation process (Pal et al., 2015).

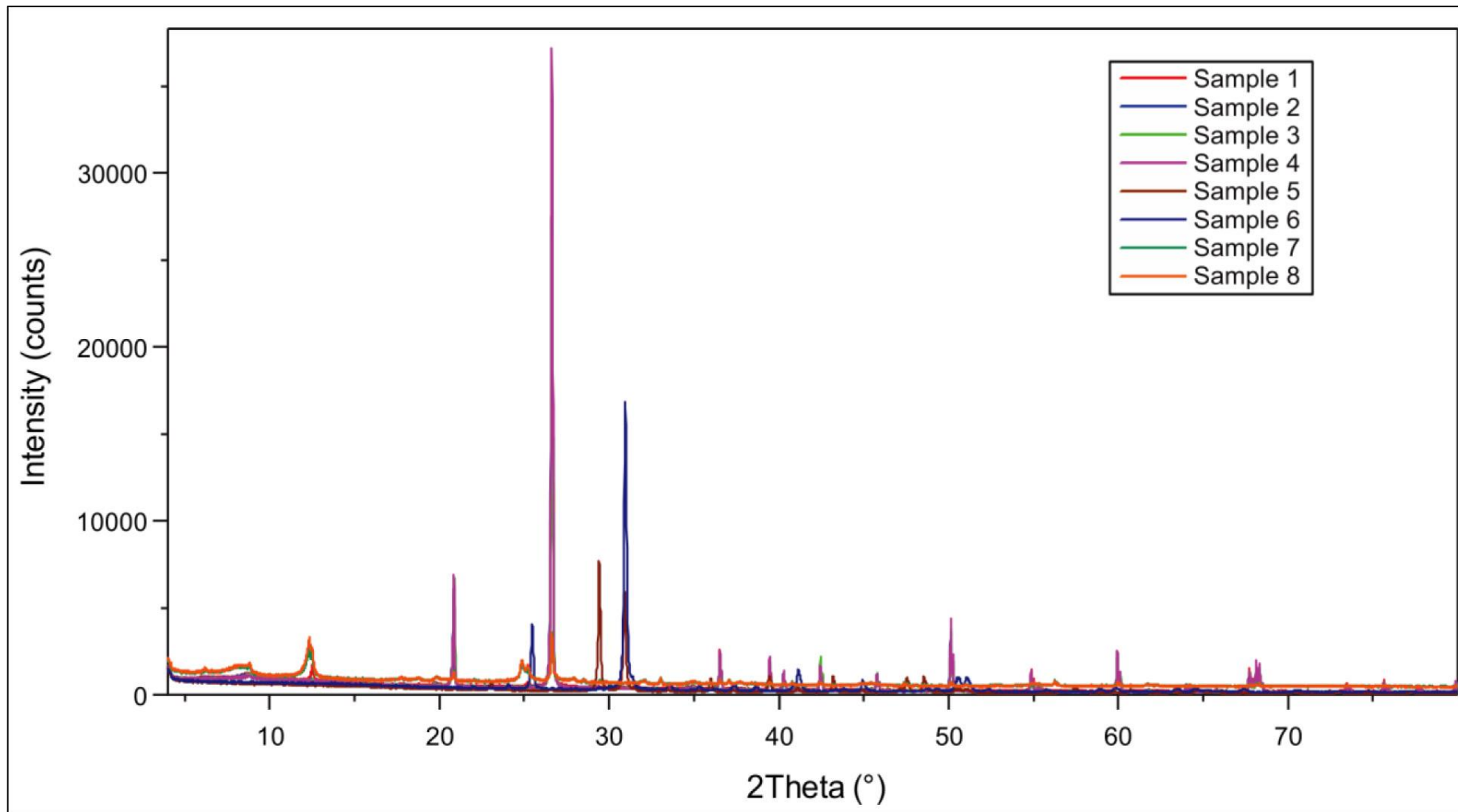


Figure 2. XRD spectrum of formation samples.

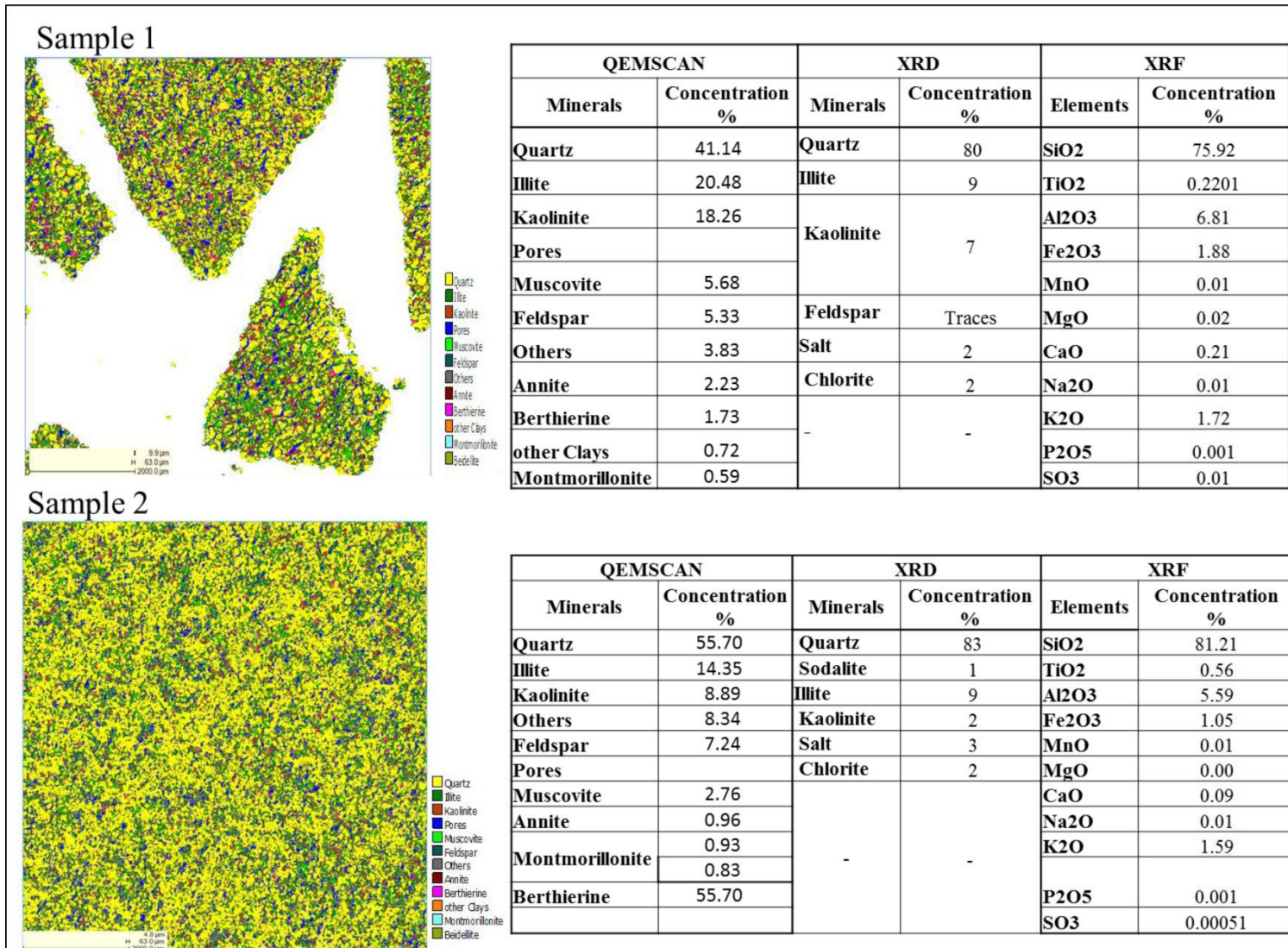
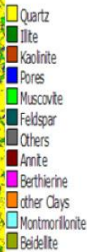
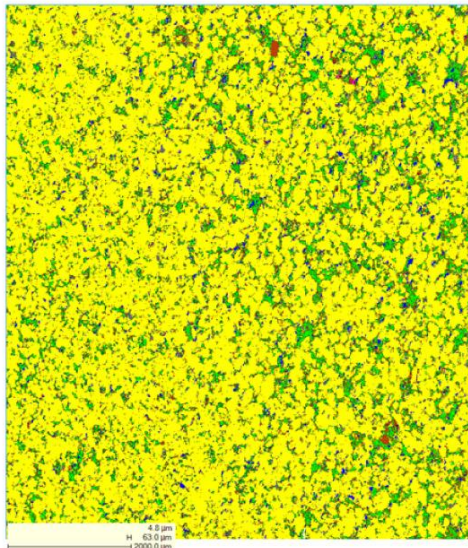


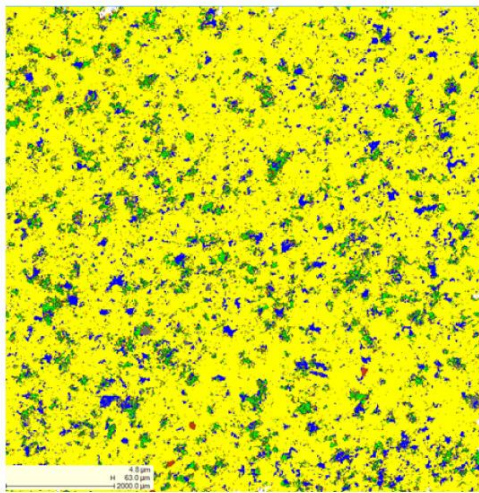
Figure 3. Quartz-rich samples exhibiting significant clay content.

Sample 3



QEMSCAN		XRD		XRF	
Minerals	Concentration %	Minerals	Concentration %	Elements	Concentration %
Quartz	74.22	Quartz	80	SiO2	84.71
Illite	6.8	Illite	14	TiO2	0.24
Kaolinite	6.53	Kaolinite	4	Al2O3	5.62
Muscovite	4.99	Salt	Traces	Fe2O3	0.99
Others	3.17	-	-	MnO	0.00
Feldspar	2.41			MgO	0.00
Pores	1.34			CaO	0.11
Montmorillonite	0.26			Na2O	0.01
Annite	0.22			K2O	1.52
Other Clays	0.03			P2O5	0.001
				SO3	0.00051

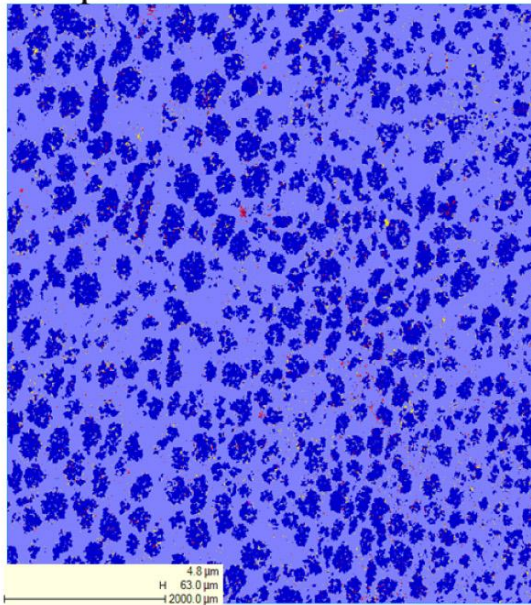
Sample 4



QEMSCAN		XRD		XRF	
Minerals	Concentration %	Minerals	Concentration %	Elements	Concentration %
Quartz	79.97	Quartz	89	SiO2	93.49
Pores	5.5	Illite	8	TiO2	0.15
Illite	4.37	Feldspar	1	Al2O3	4.05
Kaolinite	3.47	Kaolinite	2	Fe2O3	0.80
Others	2.92	-	-	MnO	0.00
Feldspar	1.85			MgO	0.00
Muscovite	1.76			CaO	0.11
Montmorillonite	0.13			Na2O	0.01
Annite	0.01			K2O	1.15
				P2O5	0.00
				SO3	0.01

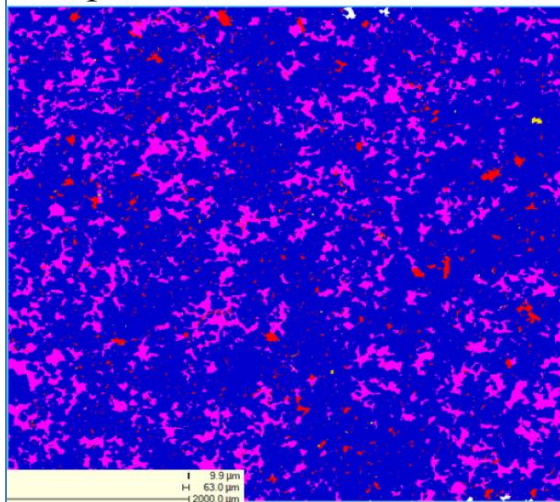
Figure 4. Quartz-rich sample exhibiting clay content.

Sample 5



QEMSCAN		XRD		XRF	
Minerals	Concentration %	Minerals	Concentration %	Elements	Concentration %
Calcite	63.6	Calcite	54	SiO ₂	6.2
Dolomite	33.96	Dolomite	45	TiO ₂	0.03
Quartz	1.28	Quartz	1	Al ₂ O ₃	1.41
Gypsum	0.13	-	-	Fe ₂ O ₃	0.49
Pores	0.07			MnO	0.01
Others	0.06			MgO	5.81
				CaO	85.52
				Na ₂ O	0.14
				K ₂ O	-
				P ₂ O ₅	0.02
				SO ₃	0.23

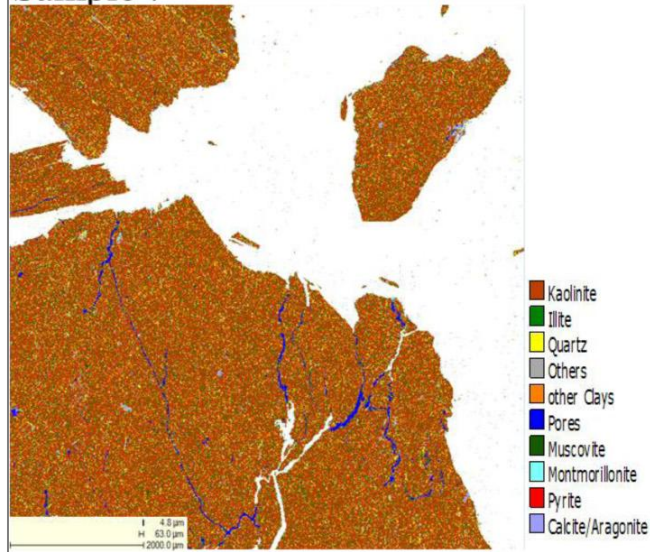
Sample 6



QEMSCAN		XRD		XRF	
Minerals	Concentration %	Minerals	Concentration %	Elements	Concentration %
Dolomite	82.28	Dolomite	75	SiO ₂	1.53
Gypsum	15.42	Gypsum	22	TiO ₂	0.01
Pores	1.14	Calcite	1	Al ₂ O ₃	0.00
Calcite	0.36	-	-	Fe ₂ O ₃	0.39
Quartz	0.09			MnO	0.01
Others	0.07			MgO	11.04
				CaO	31.28
				Na ₂ O	0.07
				K ₂ O	0.00
				P ₂ O ₅	0.001
				SO ₃	9.681

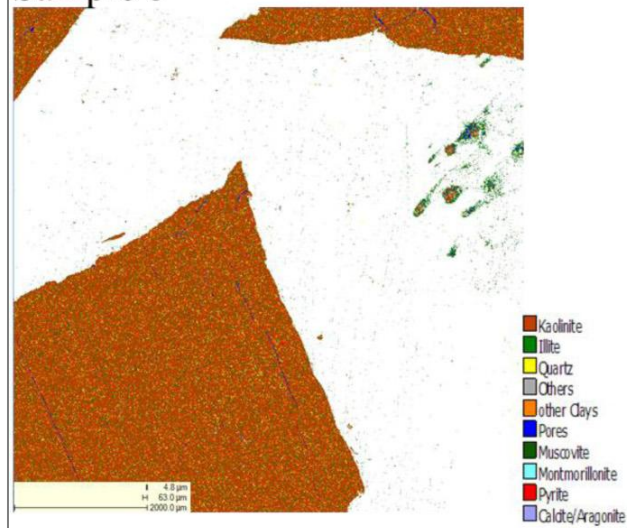
Figure 5. Carbonate-rich samples.

Sample 7



QEMSCAN		XRD		XRF	
Minerals	Concentration %	Minerals	Concentration%	Elements	Concentration %
Kaolinite	71.72	Kaolinite	50	SiO2	53.28
Illite	11.57	Illite	13	TiO2	1.18
Quartz	7.85	Quartz	20	Al2O3	24.28
Others	3.03	K-Feldspar	2	Fe2O3	11.16
other Clays	1.85	Chlorite	8	MnO	0.05
Pores	1.16	Pyrite	5	MgO	1.37
Muscovite	0.97	Na-Feldspar	2	CaO	1.95
Montmorillonite	0.85			Na2O	0.02
Pyrite	0.54			K2O	2.50
Calcite	0.47			P2O5	0.00
				SO3	4.14

Sample 8



QEMSCAN		XRD		XRF	
Minerals	Concentration %	Minerals	Concentration %	Elements	Concentration %
Kaolinite	76.34	Kaolinite	34	SiO2	44.13
Illite	11.98	Illite	9	TiO2	1.16
Quartz	4.75	Quartz	20	Al2O3	21.25
other Clays	2.11	K-Feldspar	2	Fe2O3	8.22
Others	2.08	Chlorite	16	MnO	0.03
Muscovite	1.04	Pyrite	5	MgO	1.35
Pyrite	0.63	Na-Feldspar	2	CaO	0.89
Montmorillonite	0.56			Na2O	0.01
Pores	0.48			K2O	2.19
Calcite/Aragonite	0.03			P2O5	0.057
				SO3	2.343

Figure 6. Clay-rich samples.

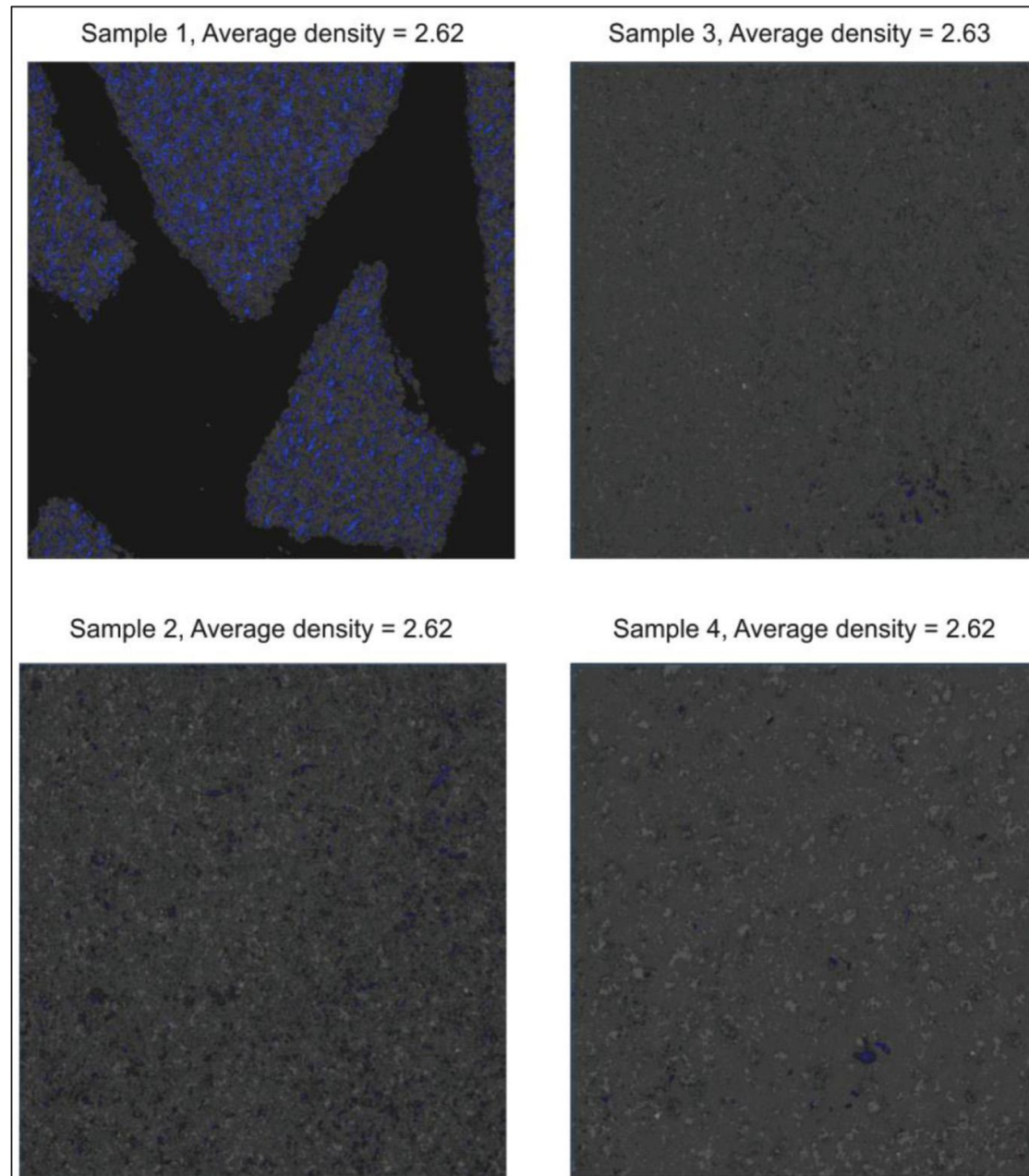


Figure 7. BSE photographs and density of quartz-rich samples.

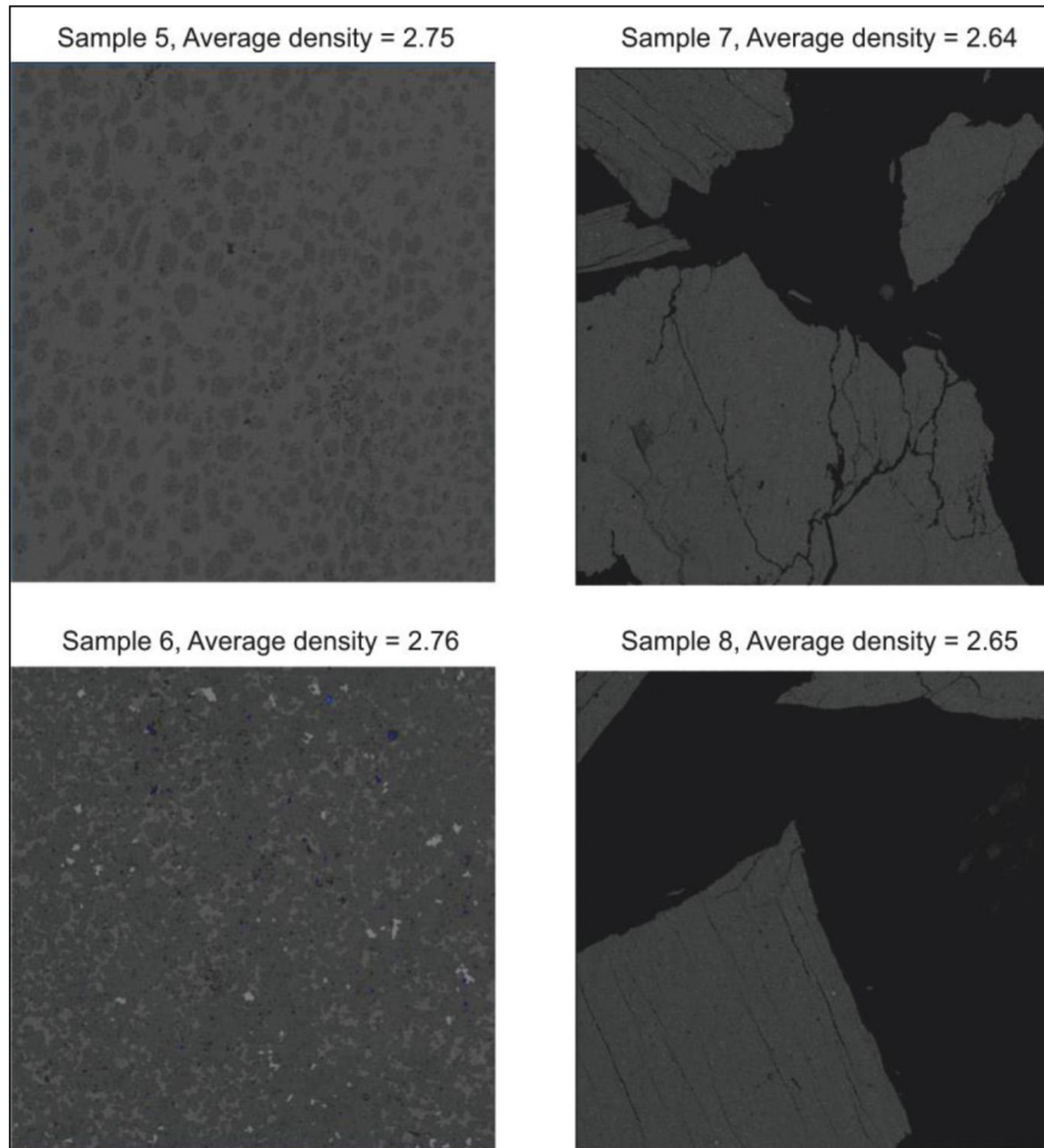


Figure 8. BSE photographs and density in carbonate- and clay-rich samples.

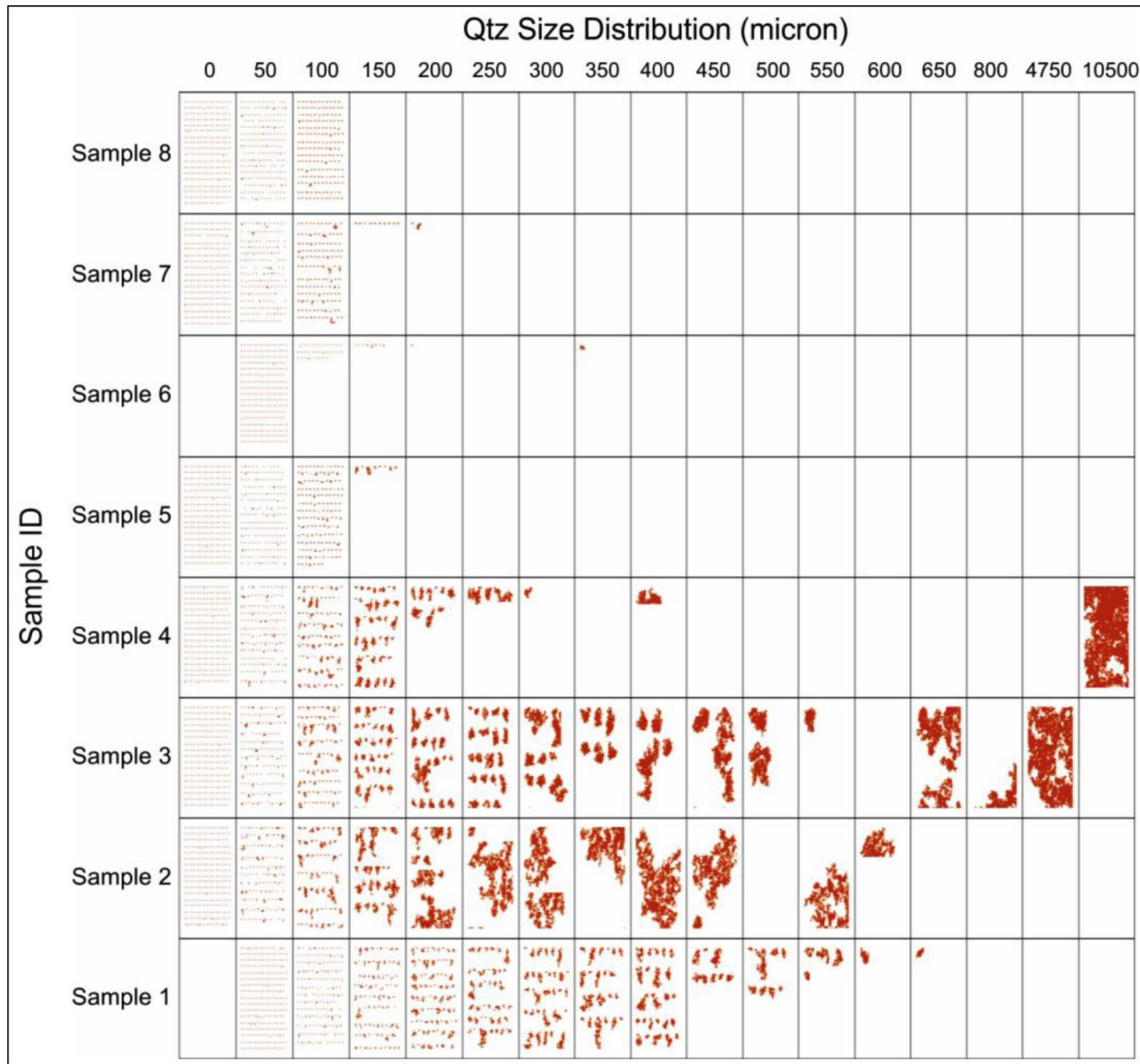


Figure 9. Grain-size distribution.